Yan *et al. Chem Synth* 2024;4:38
DOI: 10.20517/cs.2023.73

Chemical Synthesis

Research Article

Open Access

K^+ promoted fabrication of nanoneedle low-silicon ZSM-48 mesocrystal

Kexin Yan[1], Yang Zhao[1], Cheng Zhao[1], Hongbin Li[1], Zhaoqi Ye[1], Xue Yang[1], Yahong Zhang[1], Hongbin Zhang[1,2,*], Yi Tang[1,*]

[1]Department of Chemistry, Laboratory of Advanced Materials, Collaborative Innovation Center of Chemistry for Energy Materials and Shanghai Key Laboratory of Molecular Catalysis and Innovative Materials, Fudan University, Shanghai 200441, China.
[2]Institute for Preservation of Chinese Ancient Books, Fudan University Library, Fudan University, Shanghai 200441, China.

[*]**Correspondence to:** Prof. Yi Tang, Department of Chemistry, Laboratory of Advanced Materials, Collaborative Innovation Center of Chemistry for Energy Materials and Shanghai Key Laboratory of Molecular Catalysis and Innovative Materials, Fudan University, 2005 Songhu Road, Shanghai 200441, China. E-mail: yitang@fudan.edu.cn; Dr. Hongbin Zhang, Institute for Preservation of Chinese Ancient Books, Fudan University Library, Fudan University, 2005 Songhu Road, Shanghai 200441, China. E-mail: zhanghongbin@fudan.edu.cn

How to cite this article: Yan K, Zhao Y, Zhao C, Li H, Ye Z, Yang X, Zhang Y, Zhang H, Tang Y. K^+ promoted fabrication of nanoneedle low-silicon ZSM-48 mesocrystal. *Chem Synth* 2024;4:38. https://dx.doi.org/10.20517/cs.2023.73

Received: 28 Dec 2023 **First Decision:** 11 May 2024 **Revised:** 25 May 2024 **Accepted:** 11 Jun 2024 **Published:** 3 Jul 2024

Academic Editor: Jun Xu **Copy Editor:** Pei-Yun Wang **Production Editor:** Pei-Yun Wang

Abstract

Owing to their distinct structural properties, low-dimensional zeolites are rising stars in the field of catalysis. However, shortening their size while maintaining the acidity continues to be challenging. In addition, simplified synthesis methods to efficiently prepare low-dimensional zeolites with more skeleton types and extended frame components are also of great interest. Herein, a facile strategy is developed for fabricating ultrathin nanoneedle (ca. 6-8 nm in diameter of each needle) ZSM-48 mesocrystals with a low Si/Al ratio (ca. 27, close to the lowest synthesized so far). This is achieved by adding potassium ions in a ZSM-12 synthetic system. The promoting effect of appropriate K^+ ions was confirmed by adjusting the gel composition and tracking the crystallization process. Moreover, a superior conversion, reusability and regeneration performance for xylose to furfural is achieved with more accessible acidity and a more suitable Lewis/Brønsted acid ratio, which further expands the development of ZSM-48 zeolite.

Keywords: ZSM-48 zeolite, mesocrystal, morphology control, acidity, xylose dehydration

INTRODUCTION

New emerging low-dimensional zeolites, nanoscale or even < 10 nm in at least one dimension, have been considered as important catalysts due to their unique structure features[1-6]. The suitable design of low-dimensional zeolites can expand the effective accessibility of active sites while maintaining their intrinsic activity. This facilitates meeting the needs of catalytic activity, selectivity and lifetime, especially for macromolecular reactions. Nanosheets (two-dimensional)[7-11], nanorods (one-dimensional)[12-15], nanocrystals[16,17], and even subcrystals[18] (zero-dimensional) are all excellent structures that have been successfully designed. However, it is still a challenge to shorten the scale of one dimension from tens of nm to less than 10 nm under the premise of maintaining its acid properties. Besides, although some ultrathin zeolites can be directly prepared with the assistance of some structure directing agents (SDAs), such as MFI[10,19-21], MWW[7,8,22], and FER[23], and so on. So far, low-dimensional zeolites with other frameworks are still hard to construct because of the complex preparation procedure of zeolites and high cost of SDAs. Preparing low-dimensional zeolites with more frameworks using simplified synthesis methods has attracted considerable attention.

ZSM-48 zeolite is a kind of high-silicon zeolite developed by Mobil Corporation in the early 1980s. It has a one-dimensional linear channel composed of a 10-membered ring (10MR) with a diameter of 5.3 × 5.6 Å[24]. This topological feature of ZSM-48 allows it to be used in various important catalytic reactions, such as pyrolysis of alkanes[25,26], hydroisomerization of long-chain alkanes[27,28], hydrocarbon production with methanol[29], the pyrolysis of low-density polyethylene (LDPE)[30] and dehydration and isomerization of carbohydrates[31,32]. However, at present, the conventional synthesis systems of ZSM-48 are mainly divided into hexamethylenediamine (HDA) and hexamethyldiammonium (HM^{2+}). These two systems are not only prone to the existence of MFI[33] and EUO[34] impurities but also accompanied by the problem of a relatively high Si/Al ratio of final products[35]. The high Si/Al ratio of ZSM-48 (normally > 50) results in an inadequate acid density, thus limiting the reaction effect[26].

In order to solve the issues mentioned above, many approaches have been developed. Introducing crystal seed can reduce the Si/Al ratio of ZSM-48 to a certain extent[36-38]. However, zeolites with other topological structures sometimes need to be introduced as heterogeneous seeds, which increases the complexity of the synthesis process. Changing the morphology of the zeolite product to increase the external specific surface area, which can enhance the accessibility of acidic sites, is also a method to improve the catalytic performance. Constructing hollow[39], nest-like[40] or lamellar[41] structures all showed excellent results, but it requires a cumbersome post-treatment process[30,39] or elaborate and expensive SDA designs[35,42]. Therefore, it remains an urgent problem for ZSM-48 zeolite synthesis to seek a simple means that can both adjust the morphology of ZSM-48 to improve the accessibility of acidic sites and reduce the Si/Al ratio to increase the amounts of active sites.

On the other hand, adding ionic zeolite growth modifiers (ZGM), mainly alkali metal ions (such as Na^+, K^+, *etc.*), into the zeolite synthesis system can change the crystallization behavior of zeolite[23,43,44], making it a cheap and facile method to adjust the morphology of zeolite. However, this strategy of optimizing morphology has not been used in the ZSM-48 synthesis.

In this context, ZSM-48 mesocrystal with ultrathin nanoneedle morphology was prepared by adding potassium ions into the existing ZSM-12 growth system without redesigning a new SDA. Among the multistage porous ZSM-48 synthesized with template agents so far[35,40,41,45], the Si/Al ratio of this nanoneedle product is close to the lowest in the existing literature[46]. It also displays a highly catalytic performance and a relatively long lifetime for conversion of xylose to furfural reaction.

EXPERIMENTAL

Materials

To prepare organic SDA, 1,6-dibromohexane (97%, Aladdin), methanol [analytical reagent (AR), Sinopharm Chemical Reagent Co., Ltd] and 1-methylpyrrolidine (98%, Aladdin) were employed. KCl (AR, Sinopharm Chemical Reagent Co., Ltd), NaOH (AR, Sinopharm Chemical Reagent Co., Ltd), $Al_2(SO_4)_3 \cdot 18H_2O$ (AR, Sinopharm Chemical Reagent Co., Ltd) and silica sol solution (40% in water, LUDOX HS-40) were used for preparing zeolite samples. NH_4NO_3 (AR, Sinopharm Chemical Reagent Co., Ltd) was used to treat zeolite samples. Xylose (AR, Aladdin) and the commercial ZSM-48 catalyst (Catalyst Plant of Nankai University) were employed in catalytic performance evaluations.

Synthesis of organic structure directing agent

The SDA was prepared as follows: 0.25 mol of 1,6-dibromohexane was added into a three-necked flask with 150 mL of methanol, and then 0.51 mol of 1-methylpyrrolidine was dropwise added into the above solution under stirring. Subsequently, the obtained mixture was heated to 60 °C under reflux conditions. After 72 h, the SDA power was obtained by evaporation of the organic solvent followed by recrystallization with hot methanol. Its purity was confirmed through a ^{13}C nuclear magnetic resonance (NMR) experiment.

Preparation and treatment of ultrathin nanoneedle ZSM-48

Nanoneedle ZSM-48 and other zeolite samples mentioned were prepared as the following molar ratio: 30 SiO_2 : 0.25 Al_2O_3 : 7.5 NaOH : 1.5 SDA : 1,200 H_2O : 0-9 KCl (or other modifiers). In detail, 1.30 g SDA was added to 39.49 g deionized water and stirred until the SDA completely dissolved. Keep stirring conditions, then add 0.63 g NaOH, 0.3 g $Al_2(SO_4)_3 \cdot 18H_2O$ and the specified amount of modifier successively. After all the solid completely dissolved, 9.46 g silica sol was dripped into the mixture. After aging for 3 h under stirring, the obtained sol solution was transferred into a 25 mL Teflon-lined autoclave and sealed. Then, it was heated to 160 °C for 36-48 h under static conditions. Finally, the product was recovered by centrifugation, washed with deionized water and dried overnight at 80 °C. In order to remove the SDA, the obtained sample is calcined at 550 °C in air for 6 h. The H-type zeolite was obtained by ion exchange with 1 M NH_4NO_3 at 80 °C three times, followed by calcination at 550 °C for 6 h.

Catalytic performance evaluations

The conversion of xylose to furfural reactions was conducted in a 25 mL autoclave at 170 °C under rotation. For a typical run, 0.08 g xylose was added into 4.0 g deionized water. After stirring for 5 min, 0.48 g zeolite catalyst was added into the above mixture. Subsequently, the mixture was sealed and reacted at 170 °C for 6 h. After cooling to room temperature, the supernatant was separated by centrifugation, and the product was analyzed by high-performance liquid chromatography (HPLC) with a Shodex SC1011 capillary column and a refractive index (RI) detector.

In the reuse test of the catalyst, the reaction mixture is centrifuged for 5 min at 1,000 rpm to collect the underlying solid catalyst. After drying at 80 °C, the catalyst was added to the xylose solution again for the next cycle reaction. In the catalyst regeneration test, a Muffle furnace was used to calcinate the waste catalyst in an air atmosphere at 550 °C for 6 h. After cooling to room temperature, the calcined catalyst is used again for the reaction.

Characterization methods

The framework of the obtained product was confirmed by an X-ray diffraction (XRD) experiment on a Bruker D2 instrument with Cu Kα radiation.

Scanning (SEM) and transmission electron microscope (TEM) experiments were performed on a Hitachi S-4800 equipment and FEI Tecnai G2 F20 S-Twin instrument, respectively.

The ^{13}C, ^{28}Si and ^{27}Al magic angle spinning NMR spectra (MAS NMR) of the zeolite samples before calcination were collected on a Bruker AV500 spectrometer.

The framework vibration of nanoneedle zeolite is obtained by Fourier transform infrared (FT-IR) spectroscopy on a PerkinElmer spectrometer.

After the sample was activated at 300 °C under vacuum for 7 h, a Nitrogen adsorption experiment was conducted on an autosorb iQ2 at 77 K.

The thermogravimetric analysis (TGA) curve was collected on a SDT Q600 thermal analysis instrument. The analysis was carried out in an air atmosphere with a flow rate of 100 mL/min; the temperature was raised to 900 °C at a heating rate of 10 °C/min.

FT-IR spectra of adsorbed pyridine (Py-IR) were attained using a Bruker Invenio S. The sample needs to be pre-dehydrated at 450 °C in vacuum for 2 h, exposed to pyridine vapor, then pumped to remove the physical adsorption of pyridine, and measured at 150 and 450 °C.

NH_3-temperature programmed desorption (TPD) experiment was conducted on a Micromeritics AutoChem II 2920 instrument. In a typical run, a 100 mg sample was weighed and placed in the reaction tube. The sample was then heated at 10 °C/min from room temperature to 550 °C for drying pre-treatment. He flow (50 mL/min) was purged for 1 h, cooled to 100 °C, and 10% NH_3/He mixture (50 mL/min) was injected for 1 h to saturation. Switching He flow (50 mL/min) to purge for 1 h to remove the weak physical adsorption of NH_3 on the surface, followed by desorption at a warming rate of 10 °C/min at 650 °C in He atmosphere. Thermal conductivity detector (TCD) was used to detect the removed gas.

RESULTS AND DISCUSSION

Morphology and characteristics of the nanoneedle product

Firstly, all the samples obtained after adjusting the synthesis conditions are shown in Table 1. KCl/0.2/48 is considered typical among all the samples. SEM images exhibit that the KCl/0.2/48 products are aggregated particles with a size of less than 1 μm, and almost no impurity or amorphous substance can be observed [Supplementary Figure 1A and B].

Moreover, the rough surface of the aggregated particles is observed from a high-resolution SEM (HRSEM) image [Figure 1A], and the particles are composed of several very thin nanoneedles. A TEM is further employed to examine the morphology and inner structure of KCl/0.2/48. It is clear that the tail ends of the particles are nanoneedles [Figure 1B and Supplementary Figure 1C], especially the width of each nanoneedle is shortened to only ca. 6-8 nm (Figure 1B inset). Furthermore, the obvious lattice fringes can be identified from a high-resolution TEM (HRTEM) image [Figure 1C], implying the crystalline features of the as-synthesized zeolite products. In addition, after slicing KCl/0.2/48, the TEM images show that the inner of the particles also consists of some thin nanoneedles. The ordered lattice fringes and evident mesopores can be discerned from its HRTEM image [Supplementary Figure 2]. The framework of the obtained product is confirmed by XRD, which shows typical diffraction peaks of ZSM-48 zeolite. However, the peaks were relatively weakened and widened [Figure 1D] than normal commercial ZSM-48 [Supplementary Figure 3A]. It may be because the ultrathin morphology of KCl/0.2/48 is much thinner than commercial ZSM-48

Table 1. All samples obtained by adjusting synthesis conditions

Modifier	Modifier/Si	Crystallization time (h)	Sample name	Structure
KCl	0	48	KCl/0/48	ZSM-12
KCl	0.1	48	KCl/0.1/48	ZSM-12
KCl	0.2	48	KCl/0.2/48	ZSM-48
KCl	0.3	48	KCl/0.3/48	ZSM-48 + quartz
NaCl	0.2	48	NaCl/0.2/48	ZSM-12
LiCl	0.2	48	LiCl/0.2/48	ZSM-12 + impurity
KNO_3	0.2	48	KNO_3/0.2/48	ZSM-48
KCl	0.2	6	KCl/0.2/6	Amorphous
KCl	0.2	18	KCl/0.2/18	Amorphous
KCl	0.2	36	KCl/0.2/36	ZSM-48 + amorphous
KCl	0.2	40	KCl/0.2/40	ZSM-48 + amorphous
KCl	0.2	44	KCl/0.2/44	ZSM-48 + amorphous
KCl	0.2	46	KCl/0.2/46	ZSM-48 + amorphous
/	/	/	Commercial ZSM-48	ZSM-48

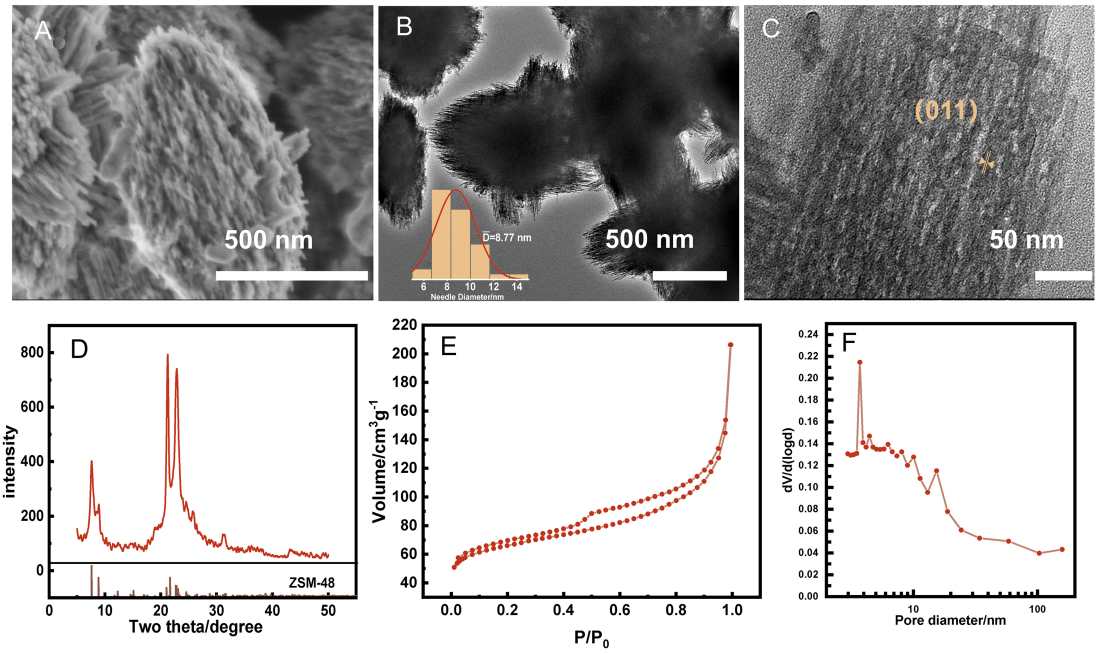

Figure 1. (A) SEM image; (B and C) TEM image, inset: the needle diameter distribution; (D) XRD pattern image; (E) N_2 adsorption isotherm of KCl/0.2/48 sample; and (F) pore size distribution in mesoporous segment. SEM: Scanning electron microscope; TEM: transmission electron microscope; XRD: X-ray diffraction.

[Supplementary Figure 3B]. FT-IR spectra analysis is further conducted to investigate the framework structure of KCl/0.2/48. Four absorption bands can be unambiguously observed at 1,214, 1,060, 785 and 545 cm^{-1} in the FT-IR spectrum [Supplementary Figure 4]. In detail, the absorption at 1,214 cm^{-1} is related to the external asymmetric stretching vibration[47,48], and the strongest absorption band at 1,060 cm^{-1} is ascribed to the internal asymmetric stretching vibration. The absorption at 785 cm^{-1} can be attributed to the external symmetric stretching vibration, and the double five-member rings result in the absorption at 545 cm^{-1}. These results demonstrate the complete ZSM-48 zeolite framework of KCl/0.2/48.

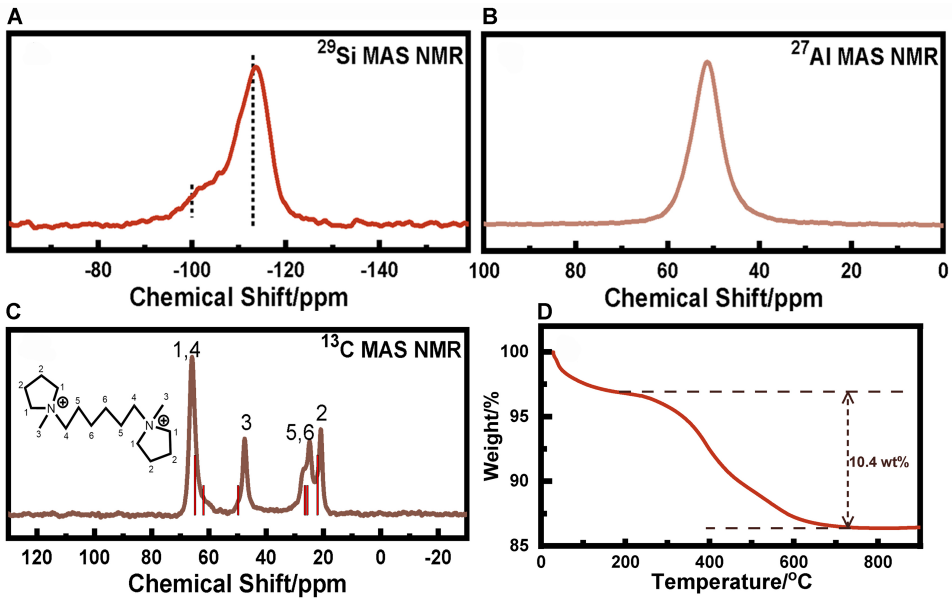

Figure 2. MAS NMR spectrum of (A) Si, (B) Al and (C) C element of KCl/0.2/48, the red bar chart is the standard ^{13}C NMR spectrum of the SDA; (D) The thermogravimetric analysis of KCl/0.2/48. MAS: Magic angle spinning; NMR: nuclear magnetic resonance; SDA: structure directing agent.

The textural property of KCl/0.2/48 is characterized by N_2 adsorption-desorption experiment. An obvious hysteresis loop at the middle relative pressure can be observed from the isotherm with the steep climb at the high relative pressure [Figure 1E], which implies the existence of mesopores, even macropores, consistent with the observation of SEM/TEM images. Moreover, the external specific surface areas are about 130 m^2/g, which can be ascribed to the very thin width of the nanoneedle. As shown in the pore size distribution of KCl/0.2/48 [Figure 1F], there are mesoporous pores between nanoneedles at about 4 nm and intercrystalline mesoporous accumulation above 10 nm. Ar adsorption-desorption experiment was also used to test the microporosity of the sample. It showed similar adsorption isotherm and mesoporous distribution, and the micropore distribution is close to that of ZSM-48 [Supplementary Figure 5].

MAS NMR is used to study the chemical environment of the components in KCl/0.2/48. Two resonances at chemical shifts of ca. -100 and -113 ppm can be detected in the ^{29}Si MAS NMR spectrum, corresponding to the Q^3 [$Si(OSi)_3OH$ or $Si(OSi)_3(OAl)$] and Q^4 [$Si(OSi)_4$], respectively [Figure 2A]. Only a signal at a chemical shift of ca. 55 ppm in the ^{27}Al MAS NMR spectrum suggests that all Al atoms are located in the zeolite framework as the tetra-coordinated form [Figure 2B]. In addition, the ^{13}C MAS NMR spectrum shows that the SDA is intact in the final product without decomposition during the hydrothermal treatment [Figure 2C]. And ca. 10.4 wt% weight loss could be detected from 200 to 750 °C in the TGA result, which corresponds to the decomposition of the template during calcination [Figure 2D]. According to the inductively coupled plasma (ICP) emission spectrometer analysis, the Si/Al ratio for KCl/0.2/48 is only ca. 27, which is comparable to the lowest value (ca. 23) reported among direct synthesis. Accordingly, it can be deduced that there is around 1 SDA molecule in each ZSM-48 zeolite unit cell.

Crystallization mechanism involving potassium ion

The decisive role of potassium ions

Generally, such a zeolite with extremely thin nanoneedles is difficult to synthesize, which means that complex bifunctional SDAs should be utilized for the preparation. However, it is hard to employ these

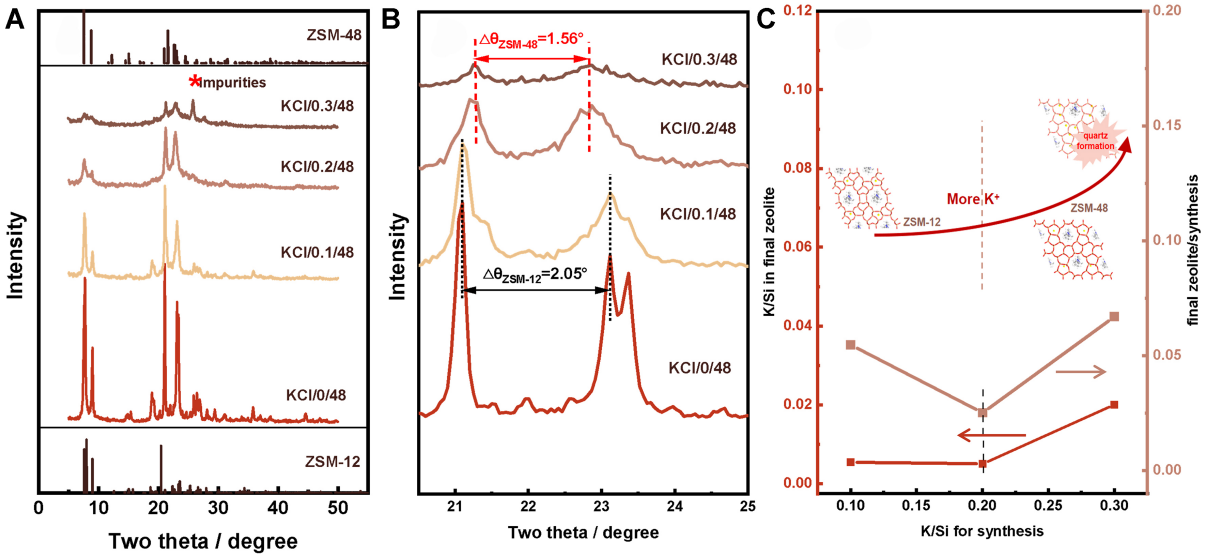

Figure 3. (A and B) XRD pattern of samples with different KCl contents; (C) the K/Si in the solid zeolite products calculated by ICP and compared with that in the initial synthetic gel, inset: diagram of correlation between product and KCl quantities. XRD: X-ray diffraction; ICP: inductively coupled plasma.

SDAs widely due to the complicated procedure for template synthesis and related high cost. Herein, we use a simple diquaternary ammonium salt as SDA combined with K^+ to facilely obtain the nanoneedle ZSM-48 mesocrystal. The high-angle annular dark field scanning transmission electron microscopy (HADDAF-STEM) images indicate that Si, Al, O and K elements are uniformly distributed in KCl/0.2/48 particles [Supplementary Figure 6]. It should be noted that KCl may play an important role in preparing nanoneedle KCl/0.2/48. If no KCl is added during the synthesis, sample KCl/0/48, an aggregated ZSM-12 zeolite with a constituting nanoparticle size of more than 30 nm, is obtained [Supplementary Figure 7A and B]. It exhibits higher peak intensities [Supplementary Figure 7C] than nanoneedle ZSM-48 zeolite in the XRD pattern due to the larger nanoparticle size. The larger nanoparticle size also corresponds to the higher adsorbed volumes of micropores in its N_2 adsorption-desorption isotherm [Supplementary Figure 7D]. This result agrees with our previous work[49].

Moreover, we adjusted the ratio of KCl and Si to obtain sample KCl/0-0.3/48 [Figure 3A]. If KCl/SiO_2 is tailored to 0.1, the intensities of peaks in XRD of KCl/0.1/48 are slightly weaker, but only the ZSM-12 zeolite framework can be obtained. However, the SEM images show both the nanoneedle ZSM-48 zeolite and ZSM-12 products in KCl/0.1/48, which were aggregated by relatively larger nanoparticles, may be generated [Supplementary Figure 8] in this situation. When KCl/SiO_2 = 0.2, the KCl/0.2/48 product of pure phase nanoneedle ZSM-48 can be obtained. This can be judged from the change in the relative distance between the two XRD characteristic peaks [Figure 3B]. If the amount of KCl is increased (KCl/SiO_2 = 0.3), some impurities of quartz gradually appear in KCl/0.3/48 product.

We also calculate the K/Si in the solid zeolite products by ICP and compare it with that in the initial synthetic gel. Dividing the K/Si of the final zeolite products by the K/Si of the initial synthetic gel, it is surprising to find that the nanoneedle sample (KCl/0.2/48) reaches the lowest ratio among all samples [Figure 3C and Table 2]. It is also found that after adding KCl, no matter whether the topological structure of the product is ZSM-12 (MTW) or ZSM-48 (*MRE), the Si/Al ratio is reduced. However, after adding potassium, the Si/Al reduction ratio for ZSM-12 is slightly greater than that of ZSM-48, which may be

Table 2. The Si/Al ratio and K content of different samples

K/Si for synthesis	Si/Al[a]	Final zeolite/synthesis	K/Si[a]
0	27.47	/	/
0.1	23.99	0.055	0.005
0.2	27.01	0.030	0.006
0.3	21.67	0.067	0.020

[a]Calculated by ICP. ICP: Inductively coupled plasma.

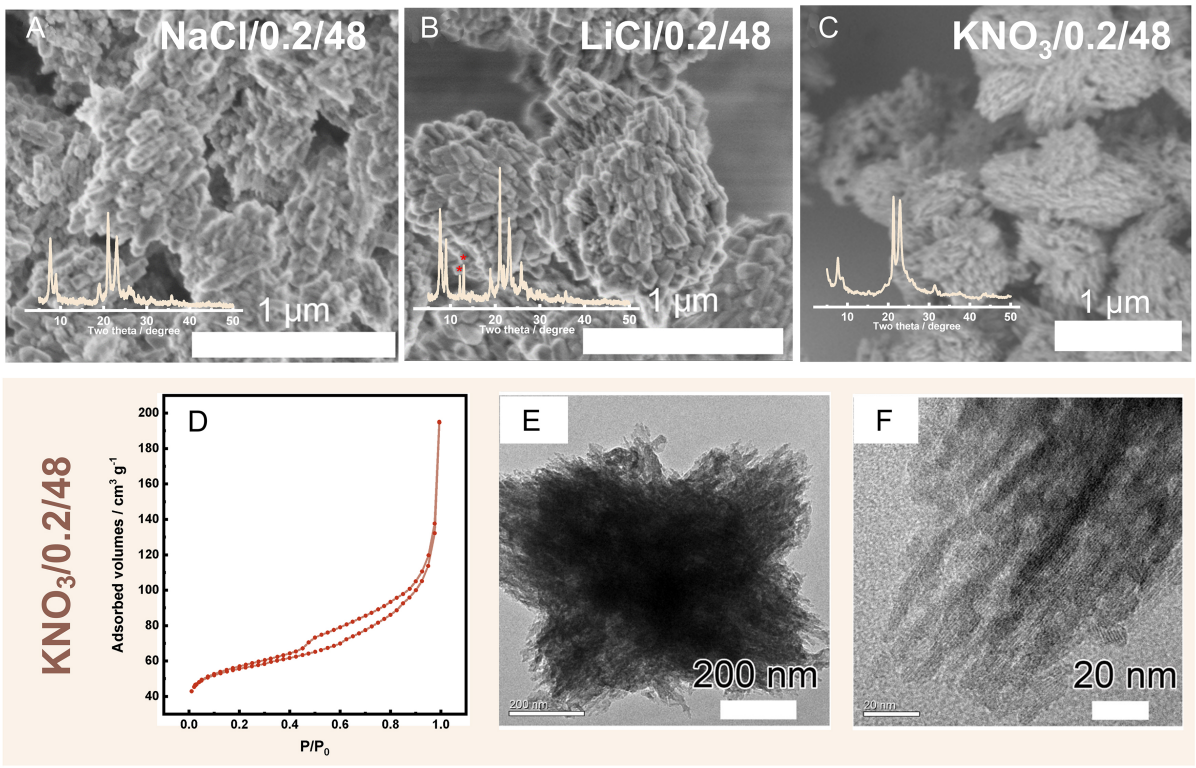

Figure 4. The SEM images of products synthesized by adding (A) NaCl, (B) LiCl and (C) KNO_3, inset: XRD pattern of products; (D) N_2 adsorption isotherm; and (E and F) TEM images of KNO_3/0.2/48. SEM: Scanning electron microscope; XRD: X-ray diffraction; TEM: transmission electron microscope.

related to the difficulty of synthesizing low-silicon ZSM-48 zeolite.

To further demonstrate the important role of potassium ions, the KCl is replaced by NaCl or LiCl. Only ZSM-12 zeolite with aggregated nanoparticles is collected [Figure 4A and B] in NaCl/0.2/48 and LiCl/0.2/48. These results imply that K^+ ions are critical for fabricating nanoneedle ZSM-48 zeolite. To further exclude the effects of anions, the KCl is replaced by KNO_3 in the synthesis system. The XRD pattern of KNO_3/0.2/48 shows that ZSM-48 zeolite is obtained with relatively lower crystallinity, and SEM images indicate that the as-prepared sample displays the nanoneedle assembled morphology [Figure 4C]. The texture information is also similar to KCl/0.2/48 [Figure 4D]. As evidently discerned in its TEM images, the width of each nanoneedle is less than 8 nm [Figure 4E and F].

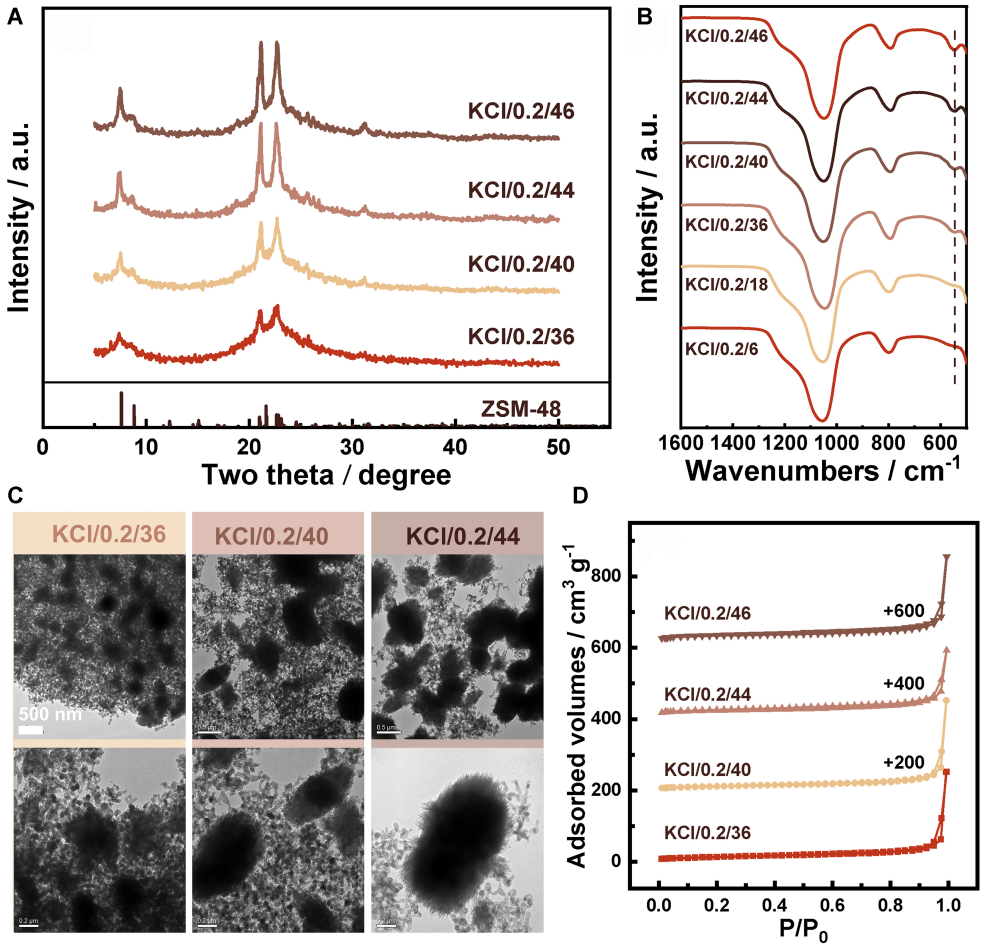

Figure 5. (A) XRD patterns; (B) FT-IR spectrums; (C) TEM images; and (D) N_2 adsorption isotherms of nanoneedle ZSM-48 zeolite at different crystallization times. XRD: X-ray diffraction; FT-IR: Fourier transform infrared; TEM: transmission electron microscope.

Time-resolved investigation on ZSM-48 crystallization

It has been proven that K^+ promotes the formation of nanoneedle ZSM-48 zeolite. Then, we further monitor the crystallization process of a typical sample to clear the exact effect of K^+. Sample KCl/0.2/X is obtained by interrupting crystallization at X hour. At about 36 h, the weak XRD characteristic diffraction peaks of ZSM-48 appear [Figure 5A], and the five-membered bands of FT-IR [Figure 5B] also indicate that the skeleton structure of zeolite begins to form. After 44 h, the XRD peak intensity of the product has not changed significantly, indicating the final crystallinity of the product has been reached.

With the extension of crystallization time from 36 to 44 h, TEM images show that the nanoneedle zeolite particles obviously increased with the continuous consumption of amorphous nanoparticles around [Figure 5C]. In particular, a large number of hollows are found in these amorphous nanoparticles [Supplementary Figure 9], which differs from the dense amorphous nanoparticles usually observed during the crystallization of zeolites. It is possible that K^+ has a destructive effect on these precursors to produce the smaller precursor nanoparticles[50]. Consequently, these smaller nanoparticles form thinner nanoneedles during the aggregation process. As a result, the width of the nanoneedle in the final product is only 6-8 nm. Besides, the N_2 adsorption isotherms [Figure 5D] show that the adsorption amount at low relative pressure gradually increases for crystallizing 36 to 46 h, indicating the increase in the volume of micropores and

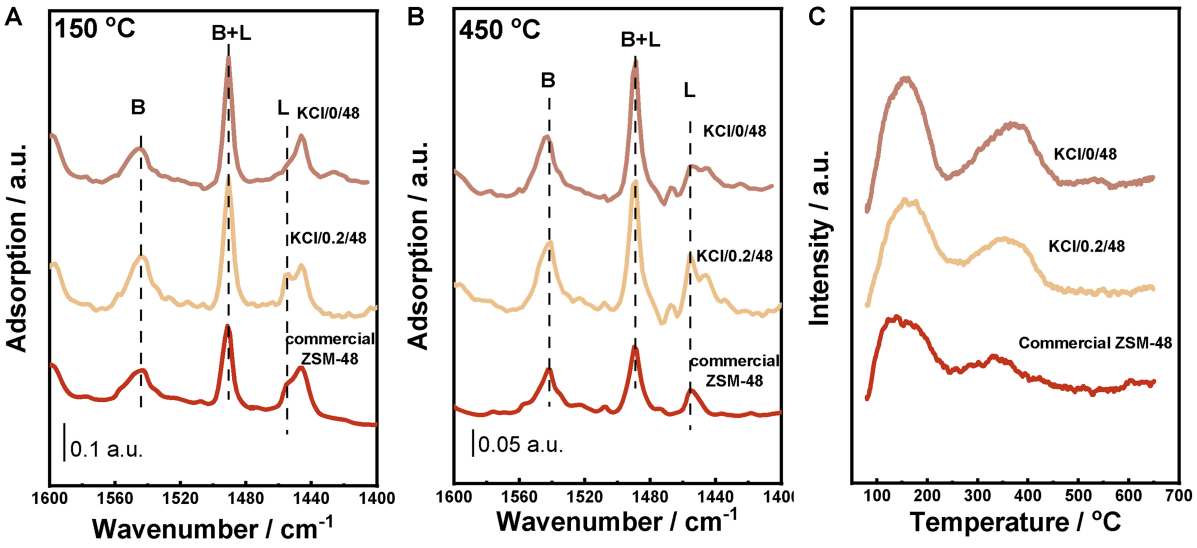

Figure 6. Py-IR spectrum at (A) 150 °C and (B) 450 °C; (C) NH_3-TPD of different catalysts. Py-IR: FT-IR spectra of adsorbed pyridine; TPD: temperature programmed desorption.

crystallinity for the intermediate products [Supplementary Table 1]. Interestingly, big hysteresis loops always exist in high-pressure regions but with a slight movement to the low-pressure direction. This suggests a process of further thinning of the nanoneedles, which are assembled from smaller pre-formed nanoparticle precursors.

Catalytic effect of xylose dehydration reaction

Because of its adjustable acidity, zeolite is widely used in synthesizing high value-added chemicals from biomass, which is of great significance for green chemistry and sustainable development. Therefore, the catalytic performance of nanoneedle KCl/0.2/48 is evaluated through xylose to furfural reaction, with commercial ZSM-48 and KCl/0/48 as benchmarks. The effect of this reaction is closely related to the acid properties of the catalysts, so we have characterized the acidity of all three catalysts.

Firstly, the results of Py-IR at 150 °C [Figure 6A] and 450 °C [Figure 6B] indicate that KCl/0.2/48 has both Lewis acid and Brønsted acid sites. Moreover, the two ZSM-48 samples have a higher L/B ratio than KCl/0/48 (ZSM-12) at both 150 and 450 °C, which may be related to the topological structure [Table 3]. The acid amount and strength of catalysts are measured by the NH_3-TPD experiment [Figure 6C]. Two distinctive desorption peaks at about 160 and 355 °C can be attributed to the weak and strong acid sites, respectively. Due to their lower Si/Al ratio, KCl/0.2/48 (0.299 mmol·g^{-1}) and KCl/0/48 (0.321 mmol·g^{-1}) have a higher total acid content than commercial ZSM-48 (0.246 mmol·g^{-1}) [Table 3]. Moreover, the amounts of weak acid sites are larger for KCl/0.2/48 (0.209 mmol·g^{-1}) than commercial ZSM-48 (0.184 mmol·g^{-1}) and KCl/0/48 (0.174 mmol·g^{-1}).

Once the nanoneedle KCl/0.2/48 is employed as the catalyst in the xylose conversion reaction [Figure 7A], the conversion of xylose greatly increases to around 95.8% [Figure 7B]. The selectivity of furfural is about 38.9% on KCl/0.2/48, while that on commercial ZSM-48 is only 13.7%. Consequently, the yield of furfural on KCl/0.2/48 (37.2%) is evidently higher than commercial ZSM-48 zeolite, which shows very low conversion (44.4%) and yield (6.1%) in this reaction. Obviously, the nanoneedle KCl/0.2/48 exhibits superiority for the conversion of xylose to furfural. This superiority is attributed not only to its more active

Table 3. Acidic properties of different catalysts

Samples	Max.temp. (°C)	Weak acid (mmol·g^{-1})	Max.temp. (°C)	Strong acid (mmol·g^{-1})	Total acid (mmol·g^{-1})	L/B[a]
Commercial ZSM-48	138.8	0.184	335.4	0.062	0.246	0.27
KCl/0.2/48	154.0	0.209	353.5	0.090	0.299	0.24
KCl/0/48	160.6	0.174	364.4	0.147	0.321	0.10

[a]Calculated by the Py-IR result of 450 °C. Py-IR: FT-IR spectra of adsorbed pyridine.

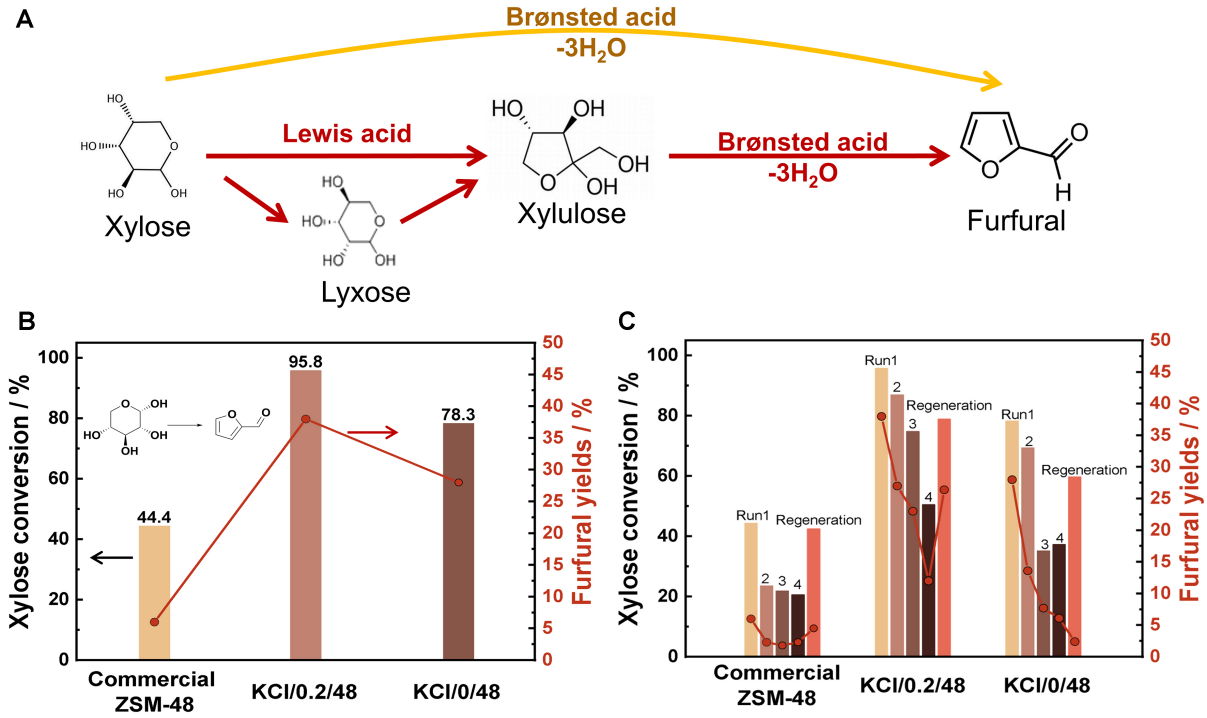

Figure 7. (A) The reaction path; (B) conversion and furfural yield; and (C) reuse and regeneration test of xylose to furfural reaction on three catalysts.

sites[51] but also to its larger external specific surface area [Supplementary Table 2], which is more conducive to the reaction on the outer surface. We also compare the KCl/0.2/48 sample with the KCl/0/48 sample aggregated by larger rods (ca. 40 nm in diameter) and find that the morphology of ultrathin nanoneedle KCl/0.2/48 (ca. 6-8 nm) still has an advantage in the reaction, although KCl/0/48 (ZSM-12) has a larger 12-membered ring channel. This may be due to not only its larger external specific surface area but also its higher L/B ratio[52,53]. Other research has shown that more Lewis acid sites will catalyze the isomerization of xylose to xylulose [Figure 7A]. The activation energy of xylulose dehydration at the Brønsted acid site (23.1 kcal/mol) is lower than that of xylulose dehydration (32 kcal/mol). Consequently, xylulose dehydrated faster than xylose itself at the Brønsted acid site[54]. Our experimental results are also consistent with this phenomenon.

The reusability and regeneration of the catalyst were also tested. After the reaction, the spent catalyst is centrifuged from the reaction liquid and added to the reaction system again. Because cokes covered the acidic sites, the catalytic effect of the three catalysts decreased to different degrees [Figure 7C]. However, KCl/0.2/48 samples showed the slowest rate of inactivation and still had a furfural yield larger than 10% after

three cycles. In comparison, the commercial ZSM-48 and KCl/0/48 samples were reduced to less than 10% furfural yield after just one cycle. Moreover, KCl/0.2/48 also showed the best catalytic effect among the three catalysts after the catalyst was regenerated by removing coke through calcination. This exhibits that the nanoneedle morphology of KCl/0.2/48 has an advantage for diffusion, which may delay the coke formation, so that the catalyst has a longer lifetime.

CONCLUSIONS

A nanoneedle ZSM-48 mesocrystal is harvested, and the width of each nanoneedle is about 6-8 nm. Meanwhile, by systematically studying morphology evolution, topological structure change, Si/Al composition, and crystallization process details, the promoting effect of K^+ has been confirmed. Furthermore, such an ultrathin ZSM-48 zeolite possesses a lower Si/Al ratio, larger external specific surface area, and more acid sites than commercial ZSM-48. It exhibits excellent catalytic performance and a long lifetime for the conversion of xylose because of more accessible acidity and a more suitable Lewis/Brønsted acid ratio. This work opens a facile and efficient avenue to fabricate low-dimensional zeolite catalysts with various frameworks, promoting the development of these materials and exhibiting great potential for improving their catalytic performance.

DECLARATIONS

Authors' contributions

Conceptualization, investigation, data curation, formal analysis, writing - original draft, visualization: Yan K
Formal analysis, validation, data curation, writing - review and editing: Zhao Y
Formal analysis, validation, data curation: Zhao C
Investigation, methodology, validation: Li H, Ye Z, Yang X
Resources, formal analysis, writing - review and editing: Zhang Y
Resources, conceptualization, formal analysis, visualization, writing - review and editing: Zhang H
Resources, formal analysis, writing - review and editing, supervision, project administration: Tang Y

Availability of data and materials

Not applicable.

Financial support and sponsorship

This work was supported by the National Key R&D Program of China (No. 2023YFA1507602) and the National Natural Science Foundation of China (Nos. 22088101, 22175040, 22072028).

Conflicts of interest

Tang Y is an Editorial Board member of the journal *Chemical Synthesis*, while the other authors have declared that they have no conflicts of interest.

Ethical approval and consent to participate

Not applicable.

Consent for publication

Not applicable.

REFERENCES

1. Přech J, Pizarro P, Serrano DP, Čejka J. From 3D to 2D zeolite catalytic materials. *Chem Soc Rev* 2018;47:8263-306. DOI PubMed
2. Xu L, Ma T, Shen Y, et al. Rational manipulation of stacking arrangements in three-dimensional zeolites built from two-dimensional zeolitic nanosheets. *Angew Chem Int Ed Engl* 2020;59:19934-9. DOI PubMed
3. Jiao M, Huang J, Xu H, et al. ECNU-36: a quasi-pure polymorph C_H beta silicate composed of hierarchical nanosheet crystals for effective VOCs adsorption. *Angew Chem Int Ed Engl* 2020;59:17291-6. DOI PubMed
4. Lei C, Dong Z, Martínez C, et al. A cationic oligomer as an organic template for direct synthesis of aluminosilicate ITH zeolite. *Angew Chem Int Ed Engl* 2020;59:15649-55. DOI PubMed
5. Guefrachi Y, Sharma G, Xu D, et al. Steam-induced coarsening of single-unit-cell MFI zeolite nanosheets and its effect on external surface Brønsted acid catalysis. *Angew Chem Int Ed Engl* 2020;59:9579-85. DOI PubMed
6. Yan K, Ye Z, Kong L, et al. Seed-induced synthesis of disc-cluster zeolite L mesocrystals with ultrashort *c*-axis: morphology control, decoupled mechanism, and enhanced adsorption. *Acta Phys Chim Sin* 2024;40:2308019. DOI
7. Luo HY, Michaelis VK, Hodges S, Griffin RG, Román-Leshkov Y. One-pot synthesis of MWW zeolite nanosheets using a rationally designed organic structure-directing agent. *Chem Sci* 2015;6:6320-4. DOI PubMed PMC
8. Chen JQ, Li YZ, Hao QQ, et al. Controlled direct synthesis of single- to multiple-layer MWW zeolite. *Natl Sci Rev* 2021;8:nwaa236. DOI PubMed PMC
9. Shen X, Mao W, Ma Y, et al. A hierarchical MFI zeolite with a two-dimensional square mesostructure. *Angew Chem Int Ed Engl* 2018;57:724-8. DOI PubMed
10. Zhang Y, Shen X, Gong Z, Han L, Sun H, Che S. Single-crystalline MFI zeolite with sheet-like mesopores layered along the a axis. *Chemistry* 2019;25:738-42. DOI PubMed
11. Tai W, Dai W, Wu G, Li L. A simple strategy for synthesis of *b*-axis-oriented MFI zeolite macro-nanosheets. *Chem Synth* 2023;3:38. DOI
12. Li B, Sun B, Qian X, et al. In-situ crystallization route to nanorod-aggregated functional ZSM-5 microspheres. *J Am Chem Soc* 2013;135:1181-4. DOI PubMed
13. Tao H, Yang H, Zhang Y, et al. Space-confined synthesis of nanorod oriented-assembled hierarchical MFI zeolite microspheres. *J Mater Chem A* 2013;1:13821. DOI
14. Ren L, Guo Q, Zhang H, et al. Organotemplate-free and one-pot fabrication of nano-rod assembled plate-like micro-sized mordenite crystals. *J Mater Chem* 2012;22:6564. DOI
15. Ye Z, Kong L, Zhao Y, et al. Alkalinity-controlled zeolite nucleation and growth: ultrafast synthesis of total-morphology zeolite L mesocrystals and adsorption evaluation. *Chem Synth* 2022;2:20. DOI
16. Awala H, Gilson JP, Retoux R, et al. Template-free nanosized faujasite-type zeolites. *Nat Mater* 2015;14:447-51. DOI PubMed
17. Yang XY, Tian G, Chen LH, et al. Well-organized zeolite nanocrystal aggregates with interconnected hierarchically micro-meso-macropore systems showing enhanced catalytic performance. *Chemistry* 2011;17:14987-95. DOI PubMed
18. Sheng Z, Li H, Du K, et al. Observing a zeolite nucleus (subcrystal) with a uniform framework structure and its oriented attachment without single-molecule addition. *Angew Chem Int Ed Engl* 2021;60:13444-51. DOI PubMed
19. Park W, Yu D, Na K, et al. Hierarchically structure-directing effect of multi-ammonium surfactants for the generation of MFI zeolite nanosheets. *Chem Mater* 2011;23:5131-7. DOI
20. Xu D, Ma Y, Jing Z, et al. π-π interaction of aromatic groups in amphiphilic molecules directing for single-crystalline mesostructured zeolite nanosheets. *Nat Commun* 2014;5:4262. DOI PubMed
21. Zhang Q, Li J, Wang X, et al. Silanol-engineered nonclassical growth of zeolite nanosheets from oriented attachment of amorphous protozeolite nanoparticles. *J Am Chem Soc* 2023;145:21231-41. DOI PubMed
22. Zhang C, Lin F, Kong L, et al. *c*-Axis-penetrated mesoporous MWW zeolite nanosheets: preparation by H_2O_2-induced micro-explosion and their enhanced properties. *Inorg Chem Front* 2022;9:4030-40. DOI
23. Lee Y, Park MB, Kim PS, et al. Synthesis and catalytic behavior of ferrierite zeolite nanoneedles. *ACS Catal* 2013;3:617-21. DOI
24. Schlenker J, Rohrbaugh W, Chu P, Valyocsik E, Kokotailo G. The framework topology of ZSM-48: a high silica zeolite. *Zeolites* 1985;5:355-8. DOI
25. Bhattacharya D, Tambe S, Sivasanker S. The influence of reaction temperature on the cracking mechanism of n-hexane over H-ZSM-48. *Appl Catal A Gen* 1997;154:139-53. DOI
26. Zhao G, Teng J, Zhang Y, et al. Synthesis of ZSM-48 zeolites and their catalytic performance in C_4-olefin cracking reactions. *Appl Catal A Gen* 2006;299:167-74. DOI
27. Mériaudeau P, Tuan VA, Nghiem VT, Sapaly G, Naccache C. Comparative evaluation of the catalytic properties of SAPO-31 and ZSM-48 for the hydroisomerization of *N-Octane*: effect of the acidity. *J Catal* 1999;185:435-44. DOI
28. Meng J, Bai D, Zeyaodong P, Li C, Chen X, Liang C. Hydroisomerization of n-hexadecane over Pt/ZSM-48 catalysts: effects of metal-acid balance and crystal morphology. *Micropor Mesopor Mat* 2022;330:111637. DOI
29. Zhang J, Huang Z, Xu L, et al. Verifying the olefin formation mechanism of the methanol-to-hydrocarbons reaction over H-ZSM-48. *Catal Sci Technol* 2019;9:2132-43. DOI
30. Azhari NJ, Mardiana S, Kadja GT. ZSM-48 zeolites with controllable mesopore formation: synthesis, characterization, and catalytic performance. *Chem Eng J Advances* 2023;16:100533. DOI

31. Kadja GTM, Azhari NJ, Mardiana S, Khalil M, Subagjo, Mahyuddin MH. Accelerated, mesoporogen-free synthesis of hierarchical nanorod ZSM-48 assisted by hydroxyl radicals. *Ind Eng Chem Res* 2021;60:17786-91. DOI
32. Saenluang K, Srisuwanno W, Salakhum S, Rodaum C, Dugkhuntod P, Wattanakit C. Nanoporous Sn-substituted ZSM-48 nanostructures for glucose isomerization. *ACS Appl Nano Mater* 2021;4:11661-73. DOI
33. Xue Y, Li S, Li J, et al. Enhancing propene selectivity in methanol and/or butene conversion by regulating channel systems over ZSM-5/ZSM-48 composite zeolites. *Micropor Mesopor Mat* 2021;312:110803. DOI
34. Giordano G, Nagy J, Derouane E. Zeolite synthesis in presence of hexamethonium ions. *J Mol Catal A Chem* 2009;305:34-9. DOI
35. Astafan A, Benghalem MA, Michelin L, et al. Synthesis of hierarchical ZSM-48 nano-zeolites. *New J Chem* 2018;42:4457-64. DOI
36. Meng J, Li C, Chen X, Song C, Liang C. Seed-assisted synthesis of ZSM-48 zeolite with low SiO_2/Al_2O_3 ratio for n-hexadecane hydroisomerization. *Micropor Mesopor Mat* 2020;309:110565. DOI
37. Shang S, Ren L, Liu Q, et al. Ultrafast synthesis and regulating Al status of mesoporous ZSM-48 zeolite via a pretreated-seed-solution-assisted strategy. *Cryst Growth Des* 2023;23:5008-18. DOI
38. Liu W, Zhang X, Yu Q, et al. Unconventional seed-assisted strategy for Al-rich hierarchical ZSM-48 zeolite. *J Colloid Interface Sci* 2024;653:1715-24. DOI PubMed
39. Liu W, Li J, Yu Q, et al. Construction of a one-dimensional Al-rich ZSM-48 zeolite with a hollow structure. *ACS Appl Mater Interfaces* 2022;14:52025-34. DOI PubMed
40. Wang R, Peng Z, Wu P, et al. Direct synthesis of nanorod stacked "nest-like" hierarchical ZSM-48 hollow spheres using a triazine-based bolaform organic structure-directing agent. *Inorg Chem Front* 2022;9:2016-22. DOI
41. Zhang Y, Ma Y, Che S. Synthesis of lamellar mesostructured ZSM-48 nanosheets. *Chem Mater* 2018;30:1839-43. DOI
42. Zhang K, Li C, Liu Z, Wang M, Yan X, Xi H. Tailoring hierarchical zeolites with designed cationic surfactants and their high catalytic performance. *Chem Asian J* 2017;12:2711-9. DOI PubMed
43. Ye Z, Zhao Y, Zhang H, et al. Mesocrystal morphology regulation by "alkali metals ion switch": re-examining zeolite nonclassical crystallization in seed-induced process. *J Colloid Interface Sci* 2022;608:1366-76. DOI PubMed
44. Lin F, Ye Z, Kong L, et al. Facile morphology and porosity regulation of zeolite ZSM-5 mesocrystals with synergistically enhanced catalytic activity and shape selectivity. *Nanomaterials* 2022;12:1601. DOI PubMed PMC
45. Liu W, Li J, Liu Z, et al. Direct preparation of *MRE zeolites with ultralarge mesoporosity: strategy and working mechanism. *ACS Appl Mater Interfaces* 2021;13:31756-65. DOI PubMed
46. Zhai M, Ding H, Zeng S, et al. Aluminous ZSM-48 zeolite synthesis using a hydroisomerization intermediate mimicking allyltrimethylammonium chloride as a structure-directing agent. *Ind Eng Chem Res* 2020;59:11139-48. DOI
47. Fan W, Li R, Ma J, Fan B, Dou T, Cao J. Crystallization mechanism study on ZSM-48 in the system Na_2O-Al_2O_3-SiO_2-$H_2N(CH_2)_6NH_2$. *Micropor Mat* 1997;8:131-40. DOI
48. Sadrara M, Khorrami MK, Darian JT, Garmarudi AB. Fabrication of highly mesoporous ZSM-48 zeolite by anionic surfactant-organosilane system for catalytic conversion of methanol to gasoline. *Solid State Sci* 2022;128:106888. DOI
49. Zhao Y, Ye Z, Wang L, et al. Engineering fractal MTW zeolite mesocrystal: particle-based dendritic growth via twinning-plane induced crystallization. *Cryst Growth Des* 2018;18:1101-8. DOI
50. Fan W, Li R, Fan B, Ma J, Cao J. Effects of introduction of different alkali metal halides on crystallization and characteristics of ZSM-48 in a solid reaction mixture system effects of alkali metal chlorides. *Appl Catal A Gen* 1996;143:299-308. DOI
51. Kim SB, You SJ, Kim YT, et al. Dehydration of D-xylose into furfural over H-zeolites. *Korean J Chem Eng* 2011;28:710-6. DOI
52. Shao Y, Sun K, Zhang L, et al. Balanced distribution of Brønsted acidic sites and Lewis acidic sites for highly selective conversion of xylose into levulinic acid/ester over Zr-beta catalysts. *Green Chem* 2019;21:6634-45. DOI
53. Valadares DS, Clemente MCH, de Freitas EF, Martins GAV, Dias JA, Dias SCL. Niobium on BEA dealuminated zeolite for high selectivity dehydration reactions of ethanol and xylose into diethyl ether and furfural. *Nanomaterials* 2020;10:1269. DOI PubMed PMC
54. Choudhary V, Sandler SI, Vlachos DG. Conversion of xylose to furfural using Lewis and Brønsted acid catalysts in aqueous media. *ACS Catal* 2012;2:2022-8. DOI